LARGE SCALE PARALLEL WAKE FIELD COMPUTATIONS FOR 3D-ACCELERATOR STRUCTURES WITH THE PBCI CODE*

E. Gjonaj#, X. Dong, R. Hampel, M. Kärkkäinen, T. Lau, W.F.O. Müller and T. Weiland
Technische Universität Darmstadt, Institut für Theorie Elektromagnetischer Felder
Schlossgartenstr. 8, 64289 Darmstadt, Germany

Abstract

A new approach for the computation of short range wake fields for ultra-relativistic bunches in linear accelerators is presented. The method is based on the time domain solution of Maxwell equations for arbitrary 3D-geometry using a purely explicit, split-operator scheme. This approach guarantees the dispersion free propagation of the numerical solution in the longitudinal direction. In addition, it enables wake field simulations on moving computational windows. These ideas have been realized in the development of PBCI; a parallelized, fully 3D-wake field code. Detailed simulation results for several accelerator components, including the TESLA 9-cell structure and a rectangular collimator used in the ILC-ESA test beam experiments are presented.

INTRODUCTION

The X-FEL and the ILC projects require high quality beams with ultra-short electron bunches. In order to predict the energy spread and emittance growth of such bunches, an accurate knowledge of the short range wake fields induced in the different accelerator components is necessary. Due to the geometrical complexity involved, however, the computation of wake fields and potentials for long accelerator structures is generally accessible only to numerical simulations.

In the course of the past 20 years, several wake field simulation codes for rotationally symmetric structures have been developed and used with considerable success in the design of linear accelerators [1, 2]. The use of a "moving window" in the simulation of ultra-relativistic bunches (Bane, Weiland [3]) and the indirect path wake potential integration (Napoly et al [4]) represent, thereby two important milestones in this development. It is, however, surprising to note that only very recently, the issue of generalizing these two approaches for simulations in 3D-geometry was addressed. In a pioneering work of Zagorodnov et al [5], a semi-implicit 3D-discretization technique for Maxwell equations with no dispersion in the longitudinal direction was introduced. This is prerequisite for a moving window implementation since in this case, the numerical phase velocity of longitudinal waves must exactly match the speed of light in vacuum. In [6], the generalization of the indirect path wake potential integration for 3D-structures was established. In [7], an eigenmode expansion approach for the computation of transition wake potentials in outgoing pipes of infinite length is proposed. Despite few differences in the implementation, the wake potential integration method used in this paper is basically the same as in [7]. The pure frequency domain description used here, however, allows for more general computations. Such a computation is, for example, the frequency domain reconstruction of the wake field solution in a beam pipe of finite length separating two inhomogeneous accelerator sections. This procedure avoids completely the time domain simulation within the separating pipe, thus, saving a considerable computation time.

In this paper, we present wake field simulations with the newly developed code **P**arallel **B**eam **C**avity **I**nteraction (PBCI) which is designed for massively parallel wake field simulations in arbitrary 3D-geometry. The algorithms used include a purely explicit and dispersion free split-operator scheme as well as a domain decomposition approach for highly balanced parallel computations. A description of these algorithms is given in first two sections. In the third section, the beam pipe termination approach based on the modal analysis of outgoing fields is presented. This approach is used, instead of the indirect path wake potential integration, for the computation of transition wake potentials in outgoing pipes of arbitrary cross section. The rest of the paper is dedicated to the numerical results obtained for a number of relevant accelerator components in the context of the X-FEL and ILC projects.

NUMERICAL METHOD

Finite Integration Technique

The general framework used in PBCI for the spatial discretization of bunch induced electromagnetic fields is the Finite Integration Technique (FIT) [8, 9]. The semidiscrete equations of FIT can be written as

$$\frac{d}{dt}\begin{pmatrix}\widehat{\mathbf{e}}\\ \widehat{\mathbf{h}}\end{pmatrix}=\begin{pmatrix}\mathbf{0} & \mathbf{M}_{\varepsilon}^{-1}\mathbf{C}^{T}\\ -\mathbf{M}_{\mu}^{-1}\mathbf{C} & \mathbf{0}\end{pmatrix}\begin{pmatrix}\widehat{\mathbf{e}}\\ \widehat{\mathbf{h}}\end{pmatrix}-\begin{pmatrix}\mathbf{M}_{\varepsilon}^{-1}\widehat{\mathbf{j}}\\ \mathbf{0}\end{pmatrix}, \qquad (1)$$

where the discrete fields $\widehat{\mathbf{e}}$ and $\widehat{\mathbf{h}}$ are interpreted as electric and magnetic voltages along the edges of a staggered discretization grid and $\widehat{\mathbf{j}}$ is the excitation current. The operator $\mathbf{C}$ denotes the topological *curl*; $\mathbf{M}_{\varepsilon}$ and $\mathbf{M}_{\mu}$ are positive definite, diagonal *material operators* allowing for the constitutive closure of the above Maxwell-Grid-Equations (MGE).

* Work partially supported by EUROTeV (RIDS-011899), EUROFEL RIDS-011935, DFG 1239/22-3 and DESY Hamburg
# gjonaj@temf.de

The integration of Eq. 1 in time is typically performed by applying an explicit time-marching scheme of the form

$$\begin{pmatrix}\hat{\mathbf{e}}\\ \hat{\mathbf{h}}\end{pmatrix}^{n+1} = \mathbf{G}(\Delta t)\bullet\begin{pmatrix}\hat{\mathbf{e}}\\ \hat{\mathbf{h}}\end{pmatrix}^{n} - \begin{pmatrix}\Delta t\mathbf{M}_{\varepsilon}^{-1}\hat{\mathbf{j}}\\ \mathbf{0}\end{pmatrix}^{n}, \qquad (2)$$

where $\mathbf{G}(\Delta t)$ represents the specific time evolution operator of the integration scheme, and $\Delta t = t^{n+1} - t^{n}$ is the integration time step. This operator, e.g., for the commonly used leapfrog integrator is given by

$$\mathbf{G}(\Delta t) = \begin{pmatrix}\mathbf{1} & \Delta t\mathbf{M}_{\varepsilon}^{-1}\mathbf{C}^{T}\\ -\Delta t\mathbf{M}_{\mu}^{-1}\mathbf{C} & \mathbf{1}-\Delta t^{2}\mathbf{M}_{\mu}^{-1}\mathbf{C}\mathbf{M}_{\varepsilon}^{-1}\mathbf{C}^{T}\end{pmatrix}. \qquad (3)$$

The leapfrog scheme has been thoroughly investigated in terms of stability and dispersion properties. In particular, for Cartesian grids it can be shown that the dispersion error is largest for waves propagating in the direction of coordinate axes (see Fig. 1a). This property of the scheme is responsible for the large dispersion error (numerical noise) which is often observed in particle beam simulations, since for these applications the longitudinal waves associated with the bunch motion dominate the electromagnetic field spectrum.

An additional drawback of the scheme is that, no moving computational window can be used in the simulation of ultra-relativistic electron bunches. Since the longitudinal phase velocity of the numerical field solution does not match the bunch velocity (moving at the speed of light in vacuum), unphysical reflections are produced at the boundaries of the computational window. These errors increase systematically with simulation time, thus deteriorating numerical accuracy, in particular, for long accelerator structures.

Split-Operator Scheme

The idea of split-operator methods is to modify the time update in Eqs. 2 and 3, such that certain, preferred spatial directions are handled separately. The split-operator scheme used in PBCI was originally developed for the purpose of suppressing numerical noise in self-consistent Particle-In-Cell (PIC) simulations [10]. It is obtained by decomposing the time evolution operator in Eq. 2 into longitudinal and transversal parts using the second order accurate, Strang splitting procedure [11]. The resulting **L**ongitudinal-**T**ransversal (LT) splitting scheme reads

$$\begin{pmatrix}\hat{\mathbf{e}}\\ \hat{\mathbf{h}}\end{pmatrix}^{n+1} = \mathbf{G}_{t}\left(\frac{\Delta t}{2}\right)\bullet\mathbf{G}_{l}(\Delta t)\bullet\mathbf{G}_{t}\left(\frac{\Delta t}{2}\right)\bullet\begin{pmatrix}\hat{\mathbf{e}}\\ \hat{\mathbf{h}}\end{pmatrix}^{n} - \begin{pmatrix}\Delta t\mathbf{M}_{\varepsilon}^{-1}\hat{\mathbf{j}}\\ \mathbf{0}\end{pmatrix}^{n}. \qquad (4)$$

The longitudinal and transversal propagators, $\mathbf{G}_{l}(\Delta t)$ and $\mathbf{G}_{t}(\Delta t)$, contain only derivatives in the longitudinal and transversal directions, respectively. Note that, the two transversal updates in Eq. 4 will not affect plane wave solutions propagating in the longitudinal direction, whereas $\mathbf{G}_{l}(\Delta t)$ represents the time evolution of a purely one dimensional system. Thus, for an appropriate choice of the time step (see below), exact numerical integration in the longitudinal direction can be arranged.

The LT scheme is completed by replacing each of the time evolution operators in Eq. 4 with second order accurate Verlet leapfrog propagators. In matrix operator form they can be written as

$$\mathbf{G}_{l;t}(\Delta t) = \begin{pmatrix}\mathbf{1}-\frac{\Delta t^{2}}{2}\mathbf{C}_{l;t}^{1}\mathbf{C}_{l;t}^{2} & \Delta t\mathbf{C}_{l;t}^{1}-\frac{\Delta t^{3}}{4}\mathbf{C}_{l;t}^{1}\mathbf{C}_{l;t}^{2}\mathbf{C}_{l;t}^{1}\\ -\Delta t\mathbf{C}_{l;t}^{2} & \mathbf{1}-\frac{\Delta t^{2}}{2}\mathbf{C}_{l;t}^{2}\mathbf{C}_{l;t}^{1}\end{pmatrix}, \qquad (5)$$

where $\mathbf{C}_{l;t}^{1} = \mathbf{M}_{\varepsilon}^{-1}\mathbf{C}_{l;t}^{T}$, $\mathbf{C}_{l;t}^{2} = \mathbf{M}_{\mu}^{-1}\mathbf{C}_{l;t}$, and $\mathbf{C}_{l}$, $\mathbf{C}_{t}$ denote the reduced *curl* operators containing only longitudinal and transversal derivatives, respectively. The overall accuracy of the above method is of second order in space and time. In addition, for a homogeneous discretization in the longitudinal direction, the scheme is stable at the "magic time step" for the one dimensional Maxwell equations, $\Delta t = \Delta z / c$, where Δz is the grid spacing in the longitudinal direction.

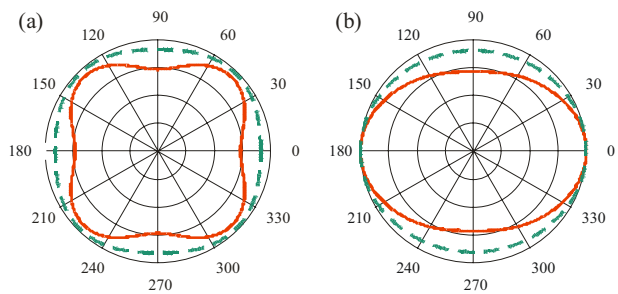

Figure 1: Normalized numerical phase velocities for the (a) leapfrog and (b) LT schemes. The deviation of the curves from the unit circle represents the dispersion error for a given propagation direction. The solid and dashed lines show the phase velocities for a grid resolution of 5 and 10 grid points per wave length, respectively. For the LT scheme $\Delta t = \Delta z / c$ is chosen.

Exact numerical dispersion relations for the LT scheme using von Neumann analysis have been derived in [10]. Here, we only show the behaviour of the numerical phase velocity as compared to the standard leapfrog scheme. Figure 1 shows normalized numerical phase velocities, which are computed from the dispersion relations as, $v = \omega/(ck)$, where ω and k are the numerical frequency and wave number, respectively, and c is the speed of light in vacuum. In each of the two graphs, two different grid resolutions for waves propagating in the *xz*-plane have been used. The dispersion error of the leapfrog scheme becomes largest in the directions of coordinate axes. Contrary, the LT-scheme (Fig. 1b) minimizes the dispersion error in the longitudinal, *z*-direction. Thus, the

effect of the above operator splitting consists in rotating the optimum dispersion direction in the longitudinal direction, corresponding to the bunch motion.

At the "magic time step", $\Delta t = \Delta z / c$, the LT scheme has no numerical dispersion along the z-direction (see Fig. 1b). The exact propagation of longitudinal waves allows for a moving window implementation. Additionally, Eq. 4 is purely explicit in time which makes the time stepping algorithm highly parallelizable.

PARALLELIZATION PROCEDURE

In fully 3D simulations involving short bunches (e.g., 300μm for the ILC-ESA experiments) and structures of several meters length, huge computational resources in terms of memory and CPU time are needed. Such simulations can only be handled in a parallel computing environment. The parallelization model used in PBCI is based on the distribution of computational tasks among a number of memory independent processing nodes. For simulation efficiency, however, well balanced workloads should be assigned to each process in order to ensure coherency in parallel program execution. Additionally, the necessary interprocess communication must be kept at the lowest level possible.

PBCI uses a geometrical decomposition of the computational domain (partitioning) between the single processes. Each processing node is responsible for performing computational tasks on the field data contained within the respective subdomain. The partitioning approach is shown schematically in Fig. 2 for a three-node cluster. Starting with the global computational domain, an orthogonal bisection of the domain bounds is recursively applied. The procedure results in a binary tree, whose internal nodes are intermediate subdomains whereas the tree leaf nodes correspond to the active (computational) subdomains. Because of the local nature of the FIT discrete operators, only field values residing at active subdomain boundaries need to be exchanged during the computation. The orthogonal bisection approach minimizes the number of such boundary values and, thus, the communication overhead in the field update equations.

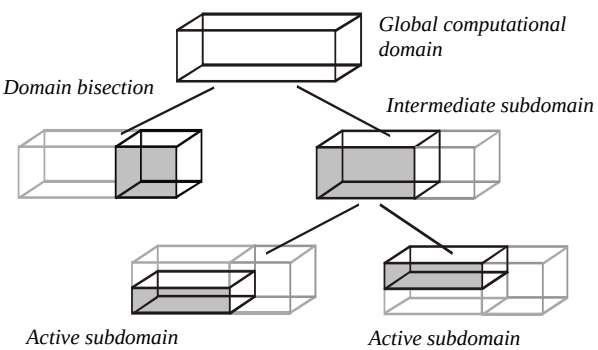

Figure 2: Example decomposition of the computational domain on a three-node cluster.

In order to determine the optimum partitioning which results in equally balanced workloads among the processing nodes, PBCI implements the load balancing scheme proposed in [12] for PIC simulations. The recursive bisection procedure is performed on the basis of computational weights W_i which are assigned to each grid point. The total computational load associated with an intermediate subdomain is, $W \sim \sum W_i$, where the summation includes only grid points within the subdomain. If the subdomain has to be partitioned between N processes, the bisection bounds are chosen such that

$$\frac{W_{\text{left}}}{W_{\text{right}}} = \frac{N_{\text{left}}}{N_{\text{right}}} \quad \text{with} \quad N_{\text{left}} = \left\lceil \frac{N}{2} \right\rceil , \; N_{\text{right}} = \left\lfloor \frac{N}{2} \right\rfloor \qquad (6)$$

where W_{left}, W_{right} and N_{left}, N_{right} are the computational weights and the number of processes, respectively, assigned to the two subdomains created by subdivision. This algorithm allows for an almost ideally balanced distribution of computational workloads. In addition, it can be applied to simulations involving an arbitrary number of processors on heterogeneous clusters.

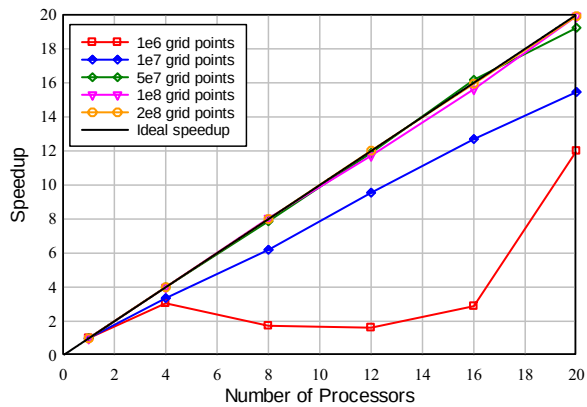

Figure 3: Parallel speedup of the algorithm for different sizes of the computational grid.

The performance of the above algorithm in terms of parallel speedup for different grid sizes is demonstrated in Fig. 3. The speedup curves show perfect behaviour, lying almost on the theoretical limit. Exceptions make the "tiny" discrete models of 1E6 and 1E7 grid cells, respectively. As expected, for these models, interprocess communication and memory cache effects dominate the computational costs. The performance tests in Fig. 3 were performed on a cluster of 3.4GHz Intel processors connected by a conventional 1Gbit/s Ethernet network.

MODAL ANALYSIS IN BEAM PIPES

For ultra-relativistic electron bunches the wake fields generated by a geometrical discontinuity of the accelerator walls will *catch-up* the bunch at a very large

distance (time) behind the discontinuity. The integral quantity of interest is the longitudinal wake potential,

$$W_z(s,z) = -\frac{1}{Q}\int_{-\infty}^{z} dz' E_z\left(x,y,z',t=\frac{z'+s}{c}\right), \quad (7)$$

where E_z is the longitudinal electric field component, s is the distance from the bunch head and z denotes the travelling distance of the bunch within the structure. The overall wake field force on the electron bunch is, then, given by $W_z(s,\infty)$. The direct integration of Eq. 7 in the time domain, however, is often impossible, because of the large *catch-up* distance behind the discontinuity.

The simple approach used in PBCI for overcoming this difficulty is schematically shown in Fig. 4. The total wake potential is separated into a "direct part", $W_z(s,0)$, containing the incoming beam pipe and the discontinuity, and a "transient part", accounting for the wake field force in the outgoing beam pipe. The direct wake potential is integrated according to Eq. 7 using the time domain simulation data. For the computation of the transient wake potential a modal expansion of the electromagnetic field solution in a transversal plane within the outgoing pipe is performed. Denoting by $z=0$ the position of the plane the general form of such an expansion is

$$E_z(x,y,0,t) = \int_{-\infty}^{\infty} d\omega \sum_n c_n(\omega) e_z^n(x,y) \exp(i\omega t), \quad (8)$$

where $e_z^n(x,y)$, is the *n*-th (TM) eigenmode solution in the pipe and $c_n(\omega)$ is the frequency domain spectral coefficient of the mode extracted by Fourier analysis. Using Eq. 8 the integration of the wake potential contribution of a single mode within the pipe,

$$W_n(s) = \int_0^{\infty} dz' \int_{-\infty}^{\infty} d\omega\, c_n(\omega) \exp\left[ik_n(\omega)z' - i\omega\frac{z'+s}{c}\right], \quad (9)$$

is readily found to

$$W_n(s) = \int_{-\infty}^{\infty} d\omega \frac{c_n(\omega)}{i\left[\omega/c - k_n(\omega)\right]} \exp\left(-i\omega\frac{s}{c}\right), \quad (10)$$

where $k_n(\omega)$ is the wave number of the mode. The total longitudinal wake potential is, then, computed as

$$W_z(s,\infty) = W_z(s,0) - \frac{1}{Q}\sum_n e_z^n(x,y) W_n(s). \quad (11)$$

Note that, in Eq. (10) the vanishing of the wake fields at infinity is explicitly used.

From the point of view of numerical implementation, the above procedure includes the one-time solution of a 2D eigenmode problem in the outgoing pipe, the Fourier analysis of the time dependent modal coefficients and the inverse Fourier transform for computing the wake potential contributions of Eq. 10. Hereby, the number of eigenmodes used in the simulation may be critical for the validity of the results. However, since only a 2D eigenmode problem has to be solved, the calculation of a large number (several hundred) eigenmodes is always possible with a minor computational effort, in particular, in the parallel implementation of PBCI.

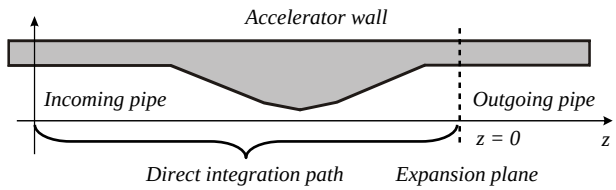

Figure 4: Separation of the wake potential computation into the direct and outgoing pipe, transition parts.

Apart from the frequency domain representation used in Eq. 10, the above procedure is equivalent to the approach proposed in [7]. The computation of the inverse Fourier transform is there avoided by introducing centred differences in time and space for the time dependent modal coefficients. Maintaining an explicit frequency domain representation of the modal coefficients, however, is of advantage for purposes other than the calculation of wake potentials. Such a situation is illustrated in Fig. 5. Shown is the PITZ diagnostics double cross [13] (see below). About one third of the structure consists of a cylindrical pipe separating a small step at the entrance from the rest of the structure. The eigenmode expansion is performed shortly behind the step. Then, using the frequency domain analysis of the modal coefficients, the full electromagnetic field solution is reconstructed within the moving window at the end of the pipe. There, the time domain simulation for the rest of the structure is resumed. This procedure results in considerable saving in the total computational time.

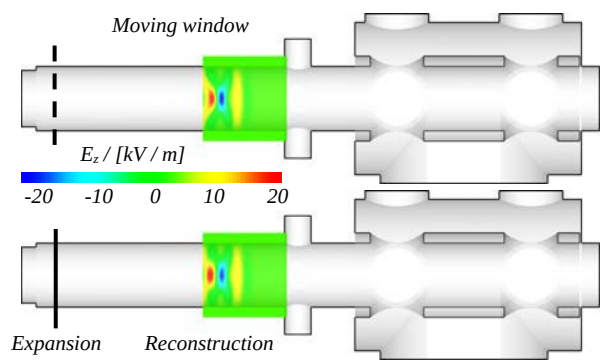

Figure 5: Time domain simulation (top) vs. frequency domain reconstruction within the moving window (bottom) in the separating pipe of PITZ. For illustration, only 15 modes were used in the reconstruction.

SIMULATION EXAMPLES

TESLA 9-Cell Structure

As a first example, the wake fields induced by a 1nC bunch of 5mm length in the TESLA 9-cell structure are presented. The simulation was performed on a moving window over a distance of 1.5m. About 80 million grid points were needed for accurately resolving geometry and bunch extension. The total simulation time for this problem size on a 24-node cluster of conventional PCs was slightly higher than 3hrs.

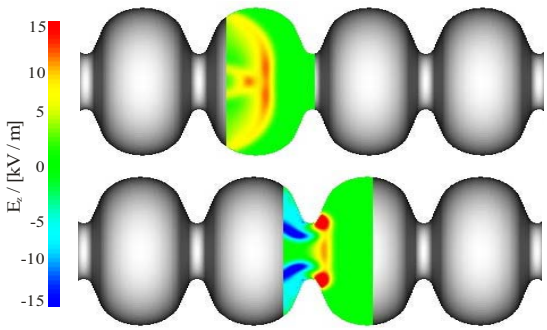

Figure 6: Geometrical view of a small section of the TESLA 9-cell structure and wake fields induced at two different bunch positions.

Figure 6 shows a 4-cell section of the structure and the wake fields within the moving window at two different bunch positions. In Fig. 7 the build-up of the longitudinal wake potential within the structure (and in part of the outgoing beam pipe) is shown. Note that, here the wake potential transition to infinity is not considered. Instead, the wake potential contributions up to different, but fixed positions within the structure are computed.

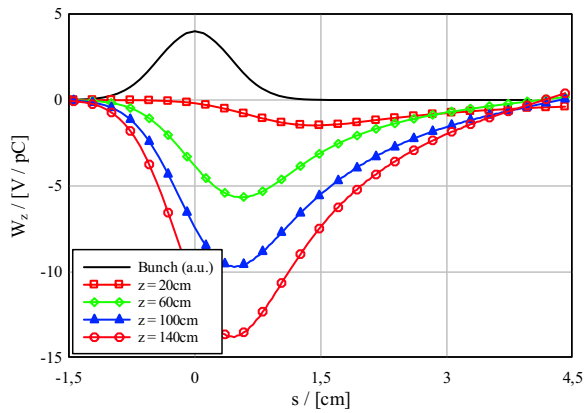

Figure 7: Build-up of the longitudinal wake potential at different positions *z* within the TESLA 9-cell structure.

Since the geometry of the TESLA 9-cell structure is (assumed) rotationally symmetric, a 2.5D simulation could have been performed. The results presented here, however, provide a good test for the performance of a fully 3D code when massive parallelization is used, even when compared to traditional 2.5D codes.

PITZ Diagnostics Double Cross Section

In this application, the wake field contributions within the diagnostics double cross of the PITZ injector [13] are computed. This section is the first part in the beam line which breaks the axis symmetry. Thus, a 3D simulation of the structure is necessary. The geometrical layout of the ten-port vacuum device is shown in Fig. 8.

The investigation includes three separate simulations for comparing the influence of the wake fields induced by the different geometrical obstacles within the device. In the first simulation, the geometry was simplified to the beam tube including only the small step at the entrance of the section. The second simulation included the vacuum vessel without the shielding tube. The third simulation considered the full geometry as shown in Fig. 8.

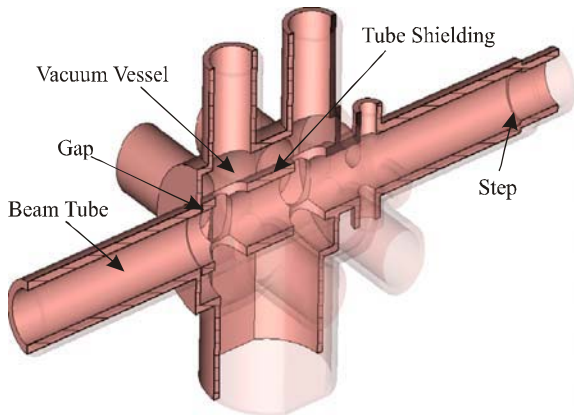

Figure 8: Geometrical view of the diagnostics double cross of the PITZ injector.

The simulation results for an electron bunch of charge 1nC and rms length 2.5mm are shown in Fig. 9. For resolving the small details of the geometry, a total of 250 million grid points were used in the discretization. It was found that the small step of 1mm height is responsible for 10-15% of the induced wake fields. The effect of the vacuum vessel inside the cross is about six times higher. The wake field effects are reduced, as expected, when the tube shielding is included.

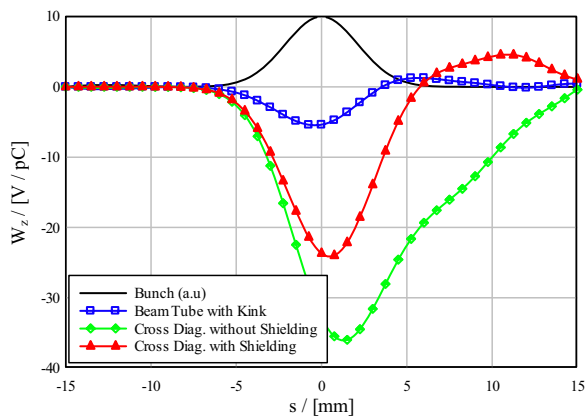

Figure 9: Longitudinal wake potentials induced by the different obstacles within the diagnostics double cross.

ILC-ESA Rectangular Collimator

The collimator considered is part of the ILC-ESA test beam program [14]. A schematic view and the dimensions of the structure are show in Fig. 10.

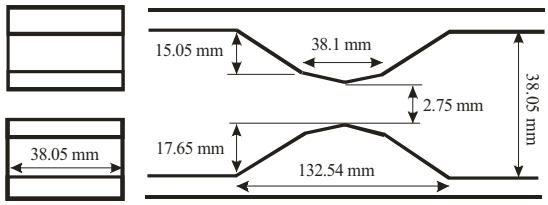

Figure 10: Beam and side views of the collimator #8 for the ILC-ESA test beam experiments.

Due to the extremely short bunch length (300μm) and the smooth tapering of the collimator slow numerical convergence is expected. Therefore, a fine discretization with a mesh resolution of up to 20μm in all three directions was used. This resulted in a computational model with more than 450 million grid points. Figure 11 shows the convergence of the longitudinal wake potential with grid resolution. Figure 12 shows the directly computed wake potential vs. the wake potential transition in the outgoing pipe. The transition potential clearly dominates the solution because of the large *catch-up* distance of the high frequency fields.

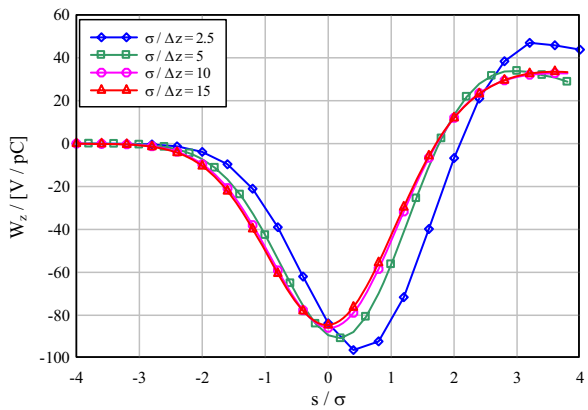

Figure 11: Convergence of the longitudinal wake potential vs. grid resolution for the ILC-ESA collimator.

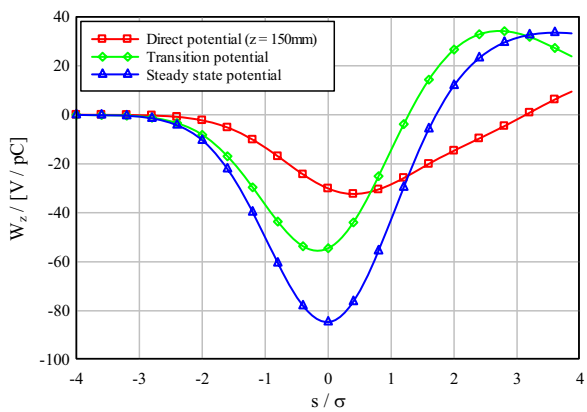

Figure 12: Direct vs. transition wake potential. 150 modes were used in the computation of the transition potential.

CONCLUSIONS

In this paper wake field simulations with the PBCI code for several X-FEL and ILC components are presented. The simulations demonstrate that the wake fields of ultra-short bunches in 3D geometry can be efficiently computed when specialized numerical algorithms combined with massive parallelization are employed.

REFERENCES

[1] T. Weiland, “TBCI and URMEL - New Computer Codes for Wake Field and Cavity Mode Calculations”, IEEE Trans. on Nucl. Sci., Vol. 30 (1983), pp. 2489

[2] I. Zagorodnov, R. Schuhmann and T. Weiland, “Long-time Numerical Computation of Electromagnetic Fields in the Vicinity of a Relativistic Source”, J. Comp. Phys., Vol. 191 (2003), pp. 525

[3] K. Bane and T. Weiland, “Wake Force Computation in the Time Domain for Long Structures“, Proc. of 12th Int. Conf. on High Energy Accel., Chicago, IL (1983), pp. 314

[4] O. Napoly, Y.H. Chin, B. Zotter, “A Generalized Method for Calculating Wake Potentials”, NIM-A, Vol. 334 (1993), pp. 255

[5] I. Zagorodnov and T. Weiland, “TE/TM Scheme for Computation of Electromagnetic Fields in Accelerators”, J. Comp. Phys., Vol. 207 (2005), pp. 69

[6] A. Henke and W. Bruns, “Calculation of Wake Potentials in General 3D Structures”, Proc. of EPAC’06, Edinburgh, UK (2006), WEPCH110

[7] I. Zagorodnov, “Indirect Methods for Wake Potential Integration,” DESY 06-081 (2006), submitted to Physical Review ST AB

[8] T. Weiland, “A Discretization Method for the Solution of Maxwell’s Equations for Six-Component Fields”, Int. J. Elect. Comm., Vol. 31 (1977), pp. 116

[9] T. Weiland, “On the Unique Numerical Solution of Maxwellian Eigenvalue problems in Three Dimensions”, Particle Accelerators (PAC), Vol. 17 (1985), pp. 227

[10] T. Lau, E. Gjonaj and T. Weiland, “Time Integration Methods for Particle Beam Simulations with the Finite Integration Technique”, FREQUENZ, Vol. 59 (2005), pp. 210

[11] G. Strang, “On the Construction and Comparison of Difference Schemes”, SIAM J. Num. Anal., 5 (1968), pp. 506

[12] F. Wolfheimer, E. Gjonaj and T. Weiland, “A Parallel 3D Particle In Cell (PIC) with Dynamic Load Balancing”, Nucl. Inst. Meth. in Phys. Res. A, Vol. 558 (2006), pp. 202

[13] A. Oppelt et al, “Status and first results from the upgraded PITZ facility” Proc. of FEL 2005, Stanford, CA (2005), pp. 564

[14] N. Watson et al., “Direct Measurement of Geometric and Resistive Wakefields in Tapered Collimators for the International Linear Collider”, Proc. EPAC’06, Edinburgh, UK (2006), MOPLS06